Bacteria primed by antimicrobial peptides develop tolerance and persist

Authors: Alexandro Rodríguez-Rojas[1§], Desiree Y. Baeder[2§], Paul Johnston[3,4], Roland R. Regoes[2]* and Jens Rolff[1,5]*.

Affiliations:

[1]Freie Universität Berlin, Institut für Biologie, Evolutionary Biology, Königin-Luise-Strasse 1-3, 14195 Berlin, Germany.

[2]Institute of Integrative Biology, Universitätsstrasse 16 ETH Zürich, 8092 Zürich, Switzerland

3. Berlin Center for Genomics in Biodiversity Research, Berlin, Germany;

4. Leibniz-Institute of Freshwater Ecology and Inland Fisheries (IGB), Berlin, Germany;

5. Berlin-Brandenburg Institute of Advanced Biodiversity Research (BBIB), Berlin, Germany

***Correspondence:** roland.regoes@env.ethz.ch, jens.rolff@fu-berlin.de,

§These authors contributed equally to this work

Key words: Antimicrobial peptides, priming, mathematical modelling, persistence, tolerance, resistance evolution

Abstract:

Bacterial resistance to drugs is a growing problem, and one that is inspiring a search for new classes of anti-bacterial compounds. This has generated interest in antimicrobial peptides (AMPs), which are key components of innate immune defences. In contrast to conventional antibiotics, however, little is known about how bacteria respond to AMPs, and whether they modify their phenotypic responses based on their prior experiences. Here, we explore whether prior exposure to sublethal doses of AMPs increases bacterial survival and abets the evolution of resistance. We show that *Escherichia coli* cells primed by sublethal doses of AMPs develop tolerance and generate more persister cells. Priming with the AMPs melittin and pexiganan leads to bacterial production of curli and colanic acid, respectively. Based on the phenotypic data we developed a population dynamic model to show how priming increases persistence and tolerance. The model predicts that priming delays the clearance of infections and fuels the evolution of genetic resistance. Since AMPs are immune effectors our results suggest that the optimal strategy to reduce problems caused by tolerant or persistent cells requires both (a) high concentrations of and (b) fast and long-lasting expression of AMPs. We anticipate that the effects discussed here will apply to many AMPs as well as other drugs that target the cell surface. Our findings also offer a new understanding of phenotypic drug resistance and could lead to measures that slow the evolution of resistance while improving the treatment of persistent infections.

Main Text:

Sublethal concentrations of antibiotics increase bacterial tolerance and persistence and therefore contribute to antibiotic resistance (*1–4*). Low, sublethal levels of antibiotics are common: whether in the environment or during medical application of antibiotics where the pharmacodynamics start at zero. While sublethal concentrations, tolerance and persistence have been of great interest for antibiotics (*1–4*), little is known about antimicrobial peptides (AMPs) which are novel drug candidates (*5*) but importantly also key effectors of innate immune defences (*6*). After infection, the induction of AMPs results in sublethal concentrations before killing concentrations are reached. But AMPs differ significantly from antibiotics in their pharmacodynamics (*7*) and they kill cells within minutes (*8*) rather than hours (*9*). Here we explore whether prior exposure to sublethal doses of AMPs increase bacterial survival and the risk of resistance, as is the case for antibiotics.

We find that a sublethal dose of certain antimicrobial peptides can induce increased tolerance and/or persistence (Fig. S1) in bacteria and hence prime (*10*) them for the exposure to a subsequent lethal dose. We identify the underlying molecular mechanisms and capture the population dynamics by adapting a classic mathematical model of persistence (*11*). With computational simulations, we then illustrate that increasing tolerance and persistence has a positive effect on bacterial survival and the emergence of resistance.

First, we studied the effect of priming *E. coli* K-12 using two antimicrobial peptides, melittin from the honeybee, and pexiganan, the first eukaryotic AMP used as a drug (*6*). We primed using a fraction of the minimal inhibitory concentration (0.1xMIC, table S1) and then monitored bacterial survival over time under lethal concentrations of the respective AMPs (10 x MIC, table S1). We found that the priming treatment resulted in much higher *E. coli* survival (Fig. 1 A, B).

The decline of the time kill curves is biphasic suggesting two subpopulations (*11–14*). We excluded that deviations from monophasic decline arise because of decreasing antimicrobial concentrations over time (Fig. S2) and fitted the time-kill curves to a biphasic linear function. For both AMPs, bacterial populations declined faster during the first than the second phase (Fig. 1, Table S2, S3). Tolerance, the decline of bacterial populations in the first phase (*4*), was significantly higher in primed than in naïve bacteria for both AMPs. Primed bacteria showed higher survival in the second phase, indicating higher numbers of persisters (*4*). The change in population size in the second phase, however, was not significantly different between primed and naïve populations, indicating that the dynamics of stochastically switching into and out of the persister state in the second phase are not influenced (Fig. 1). In short, priming with AMPs allow bacteria to survive better by increasing both bacterial tolerance and persistence.

To understand how priming leads to tolerance and persistence, we used RNAseq of cells exposed to priming concentrations of AMPs (Tables S4, 5). Melitin induced up-regulation of curli fimbriae and pexiganan induced the colanic acid synthesis (Fig. 2, S3). Curli is an important virulence factor (*15*) and component of extra-cellular matrix and protects against AMPs (*16*). Likewise, colanic acid capsules protect against AMPs and antibiotics (*17*). Both AMPs also induced significant overlap in gene expression related to osmotic shock (Fig. 2, S3). The removal of an essential gene for colonic acid production completely abolished the priming effect by pexiganan. A curli-deficient mutant showed a decrease of the priming effect induced by melittin (Fig. S4).

By phase contrast imaging, we observed the formation of a characteristic colonic acid capsule in pexiganan-primed but not in naïve cells (Fig. S5, S6) and the priming response was homogenous. For melittin primed bacteria curli induction was documented with a specific curli binding chemical (Fig. S6, S7) and this response was homogenous (Fig. S8).

Afrter lethal exposure to melittin and pexiganan we observed a high degree of heterogeneity regarding the killing rate of individual cells in primed bacteria but not in controls (Fig. S8). Primed cells also aggregate with stronger effect in pexiganan-treated cells (Fig. S8).

A decrease of intracellular ATP increases persistence under the antibiotic ciprofloxacin (*18*). Because ATP leakage is a hallmark of AMP-treated bacteria (*19*), we exposed melitin and pexiganan primed populations and controls to ciprofloxacin (*18*). This resulted in a highly significant increase in the number of persisters (Fig. S9). The level of leaked ATP in the culture supernatant was significantly higher in primed bacteria for both AMPs (Fig. S9). The pre-treatment with melittin or pexiganan does not change the MIC of *E. coli* to melittin, pexiganan or ciprofloxacin consistent with the definition of persisters (*4*) (Table S5).

To quantify the influence of priming on bacterial tolerance and persistence, phenomena inherently linked to the growth dynamics and subpopulation structure, we developed a population dynamics model that captures tolerance and persistence. We build on a two-state population model previously developed (*11*) to describe bacterial antibiotic persistence (Fig. S10). This model assumes that bacteria exist in two phenotypic states, normal cells (N) and persisters (P). The two subpopulations N and P differ in their susceptibility to AMPs, a difference that is implemented as differing net growth rates r_N and r_P, respectively. Bacteria switch from subpopulation N to P with the rate s_N and back with the rate s_P. We quantified the model parameters by fitting the analytical solution of the model equations to the time-kill datasets of melittin and pexiganan (Fig. 3A,B and Table S6). In a first fit with four free parameters (r_N, s_N, r_P, and s_P,), the parameter r_p was not significantly different from 0 (Fig. S11). In the fit with three free parameters, r_N, s_N, and s_P, priming affected the parameter r_N and s_P (Fig. S12): r_N increased due to priming,

which translates into increased tolerance (see suppl) and s_P decreased. Together, an increase in r_N and decrease in s_P result in higher persistence (Fig. 3C, D) .

To assess the influence of priming on possible treatment success and resistance evolution, we extended a previously developed predictive framework (*7*) by a persistent subpopulation (Fig. S10). We then explored the effects of priming on tolerance and persistence, individually and in combination, which would be challenging empirically. Using our predictive framework, we investigated the effect of priming on survival based on a zero-order pharmacokinetic profile (*7*, *20*) (Fig. S13) and with parameterized pharmacodynamics functions (Fig. S14).

We found that survival of the population was highly dependent on tolerance (Fig. 4A, B, S15). The presence of persistent cells alone only marginally increased time until clearance. When we implemented a decrease in switching rate s_P, the time until clearance of the bacterial population is extended at high treatment intensities (high concentrations A_{max}). The results do not qualitatively change for larger pharmacokinetic decay rates (k) typical for AMPs (Fig. S16). Taken together, an increase in tolerance alone resulted in higher survival independent of persister cells. An increase in persister cells further increased survival at high antimicrobial concentrations.

Next, we assessed how priming affects resistance emergence. Generally, resistance evolution depends on the population size, mutation rate and the replication rate. While priming increases bacterial survival, hence the population size, it also increases the number of persisters that do not replicate and hence are a poor source of resistant mutations (*11*) (Fig 1, Fig. S17). Our simulations revealed that the beneficial effects of priming on survival due to increased persistence did not translate into an increased probability of resistance emergence and establishment (Fig. 4B, S15, S16). The

probability of resistance emergence was mainly influenced by the effect of priming on tolerance.

We find that sublethal dosing of the AMPs melittin and pexiganan primes bacterial cells to increase both, tolerance and persistence. This differs from antibiotics, which usually increase either tolerance or persistence (*4*). The molecular basis of the induction of AMP tolerance and persistence relies on modifications of bacterial envelopes involving curli or colonic acid respectively. Interestingly, the activation of both pathways shows different dynamics in biofilm formation (*21*). Because curli and colanic acid are important component of the biofilm matrix, triggering their expression by sublethal levels of AMPs could potentially catalyse the biofilm formation. Within a host, if the immune system fails to clear the pathogens, the AMP-priming effect may thereby favour the transition from acute to chronic bacterial infections, where biofilms prevail.

Sublethal concentrations of antimicrobials are common and cannot only directly select for *bona fide* resistance (*22*) but can also generate phenotypic resistance indirectly (*3*). Priming by AMPs likely plays a role in infection vectors: in the flea gut the PhoQ-PhoP system is induced in *Yersinia pestis* by AMPs leading to biofilm formation that enhances transmission to the final host (*23*). It is not clear as yet if phenotypic AMP-resistance will facilitate opportunistic infections in a way similar to genetic AMP-resistance, as has been shown for *S. aureus* (*24*), but in the light of our results it seems likely. Our combined theoretical and empirical results suggest that in hosts the optimal strategy of AMP-expression requires three components: (i) high concentrations to clear bacteria quickly (ii) fast up-regulation to avoid priming and (iii) and long up-regulation to clear all of the targeted bacteria. We anticipate that these requirements also hold for the medical application of AMPs.

References and Notes:

1. D. I. Andersson, D. Hughes, Microbiological effects of sublethal levels of antibiotics. *Nat. Rev. Microbiol.* 12, 465–478 (2014).

2. B. R. Levin, D. E. Rozen, Non-inherited antibiotic resistance. *Nat. Rev. Microbiol.* 4, 556–562 (2006).

3. I. Levin-Reisman, I. Ronin, O. Gefen, I. Braniss, N. Shoresh, N. Q. Balaban, Antibiotic tolerance facilitates the evolution of resistance. *Science*. 355, 826–830 (2017).

4. N. Q. Balaban, S. Helaine, K. Lewis, M. Ackermann, B. Aldridge, D. I. Andersson, M. P. Brynildsen, D. Bumann, A. Camilli, J. J. Collins, C. Dehio, S. Fortune, J.-M. Ghigo, W.-D. Hardt, A. Harms, M. Heinemann, D. T. Hung, U. Jenal, B. R. Levin, J. Michiels, G. Storz, M.-W. Tan, T. Tenson, L. Van Melderen, A. Zinkernagel, Definitions and guidelines for research on antibiotic persistence. *Nat. Rev. Microbiol.* 17, 441–448 (2019).

5. C. D. Fjell, J. A. Hiss, R. E. W. Hancock, G. Schneider, Designing antimicrobial peptides: form follows function. *Nat. Rev. Drug Discov.* 11, 37–51 (2012).

6. M. Zasloff, Antimcirobial peptides of multicellular Organisms. *Nature*. 415, 389–395 (2002).

7. G. Yu, D. Baeder, R. Regoes, J. Rolff, Predicting Drug Resistance Evolution: Antimicrobial Peptides Vs. Antibiotics. *Proc R Soc Lond B*, 138107 (2018).

8. G. E. Fantner, R. J. Barbero, D. S. Gray, A. M. Belcher, Kinetics of antimicrobial peptide activity measured on individual bacterial cells using high-speed atomic force microscopy. *Nature Nanotech.* 5, 280-285 (2010).

9. Z. Yao, D. Kahne, R. Kishony, Distinct Single-Cell Morphological Dynamics under Beta-Lactam Antibiotics. *Mol. Cell*. 48, 705–712 (2012).

10. M. Hilker, J. Schwachtje, M. Baier, S. Balazadeh, I. Bäurle, S. Geiselhardt, D. K. Hincha, R. Kunze, B. Mueller-Roeber, M. C. Rillig, J. Rolff, T. Romeis, T. Schmülling, A. Steppuhn, J. van Dongen, S. J. Whitcomb, S. Wurst, E. Zuther, J. Kopka, Priming and memory of stress responses in organisms lacking a nervous system: Priming and memory of stress responses. *Biol. Rev.* 91, 1118–1133 (2016).

11. N. Q. Balaban, J. Merrin, R. Chait, L. Kowalik, S. Leibler, Bacterial Persistence as a Phenotypic Switch. *Science*. 305, 1622–1625 (2004).

12. A. J. Hedges, An examination of single-hit and multi-hit hypotheses in relation to the possible kinetics of colicin adsorption. *J. Theor. Biol.* 11, 383–410 (1966).

13. P. Abel Zur Wiesch, S. Abel, S. Gkotzis, P. Ocampo, J. Engelstädter, T. Hinkley, C. Magnus, M. K. Waldor, K. Udekwu, T. Cohen, Classic reaction kinetics can explain complex patterns of antibiotic action. *Sci. Transl. Med.* 7 (2015).

14. C. Wiuff, R. M. Zappala, R. R. Regoes, K. N. Garner, F. Baquero, B. R. Levin, Phenotypic Tolerance: Antibiotic Enrichment of Noninherited Resistance in Bacterial Populations. *Antimicrob. Agents Chemother.* 49, 1483–1494 (2005).

15. M. M. Barnhart, M. R. Chapman, Curli biogenesis and function. *Annu. Rev. Microbiol.* 60, 131–47 (2006).

16. S. Maria-Neto, K. C. de Almeida, M. L. R. Macedo, O. L. Franco, Understanding bacterial resistance to antimicrobial peptides: From the surface to deep inside. *Biochim. Biophys. Acta BBA - Biomembr.* 1848, 3078–3088 (2015).

17. H. Miajlovic, S. G. Smith, Bacterial self-defence: how Escherichia coli evades serum killing. *FEMS Microbiol. Lett.* 354, 1–9 (2014).

18. Y. Shan, A. Brown Gandt, S. E. Rowe, J. P. Deisinger, B. P. Conlon, K. Lewis, ATP-Dependent Persister Formation in Escherichia coli. *mBio*. 8, e02267-16 (2017).

19. K. A. Brogden, Antimicrobial peptides: pore formers or metabolic inhibitors in bacteria? *Nat. Rev. Microbiol.* 3, 238–50 (2005).

20. R. R. Regoes, C. Wiuff, R. M. Zappala, K. N. Garner, F. Baquero, B. R. Levin, Pharmacodynamic Functions: a Multiparameter Approach to the Design of Antibiotic Treatment Regimens. *Antimicrob. Agents Chemother.* 48, 3670 (2004).

21. C. Prigent-Combaret, G. Prensier, T. T. Le Thi, O. Vidal, P. Lejeune, C. Dorel, Developmental pathway for biofilm formation in curli-producing Escherichia coli strains: Role of flagella, curli and colanic acid. *Environ. Microbiol.* 2, 450–464 (2000).

22. E. Gullberg, S. Cao, O. G. Berg, C. Ilbäck, L. Sandegren, D. Hughes, D. I. Andersson, Selection of Resistant Bacteria at Very Low Antibiotic Concentrations. *PLoS Pathog.* 7, e1002158 (2011).

23. V. Vadyvaloo, A. K. Viall, C. O. Jarrett, A. K. Hinz, D. E. Sturdevant, B. J. Hinnebusch, Role of the Phop-PhoQ gene regulatory system in adaptation of yersinia pestis to environmental stress in the flea digestive tract. *Microbiol.* 161, 1198–1210 (2015).

24. G. Cheung, E. Fisher, J. McCausland, J. Choi, J. Collins, S. Dickey, M. Otto, Antimicrobial peptide resistance mechanism contributes to Staphylococcus aureus infection. *J. Infect. Dis.* 217, 1153-1159 (2018).

Acknowledgments: We are grateful to Sophie Armitage and Olivia Judson for comments on the manuscript.

Methods

Bacteria and growth conditions.

The *E. coli* MG1655 was used as bacterial models for all experiments. All cultures related to antimicrobial tests were carried out in Mueller-Hinton I Broth (Sigma). For genetic manipulations, the strain and its derivatives were routinely cultured in Lysogeny Broth (LB medium) or SOB, supplemented with antibiotics when appropriate. Other constructed and strains used in these study are listed in table X of this section.

Minimal inhibitory concentration (MIC).

MICs were determined according to CLSI recommendations by a microdilution method in MHB with some modifications. Inoculum size that was adjusted to 2×10^7 CFU/ml from a regrowth of overnight cultures to be consistent with the downstream experiments. The MIC was defined as the antimicrobial concentration that inhibited growth after 24 h of incubation in liquid MH medium at 37°C. Polypropylene non-binding plates (Th. Geyer, Germany) were used for all experiments. The MIC was considered as the antimicrobial concentration that inhibited growth after 24 hours of incubation in liquid medium at 37°C.

Priming experiments.

Starting from $1x10^8$ CFU/ml, where bacteria were exposed (stimulus) to 1/10 MIC of melittin or pexiganan during 30 minutes at 37°C with soft shaking. The tubes were centrifuged at 4000 g for 10 minutes and allow to recover during 60 minutes. The cells were challenged (trigger of priming response) with a concentration equivalent to an 10X MIC. The cultures were diluted and plated to determine cell viability. Five replicas per culture were used, and every experiment was repeated twice. Non treated cells were used as a control.

Persister Antibiotic survival assay.

Bacterial cultures were inoculated at 1:100 from a 16-hour overnight culture into MHB medium. Cell were grown during 2 h to reach approximately to 2×10^8 CFU/ml). The cultures were treated with priming concentrations (1/10 MIC) of melittin and pexiganan during 30 minutes. Non-treated cultures were used as control. All cultures were washed and centrifuged twice to remove the treatment. The supernatants were used to determine ATP concentration using a Molecular Probes ATP Determination Kit (Thermo Fisher Scientific, Germany). Bacteria were resuspended in equal volume of fresh medium and an aliquot from each culture was taken to determine the number of bacteria at t=0 by diluting and plating in MHB agar. Following, ciprofloxacin was added for a final concentration of 2 µg/ml to treated tubes and to non-treated AMPs control. The cultures were incubated during four hours. Then, bacteria were washed twice with 0.9 % NaCl and plated on MHB agar to determine the counts of survival fractions. The percent survival was calculated as the ration between described previously [1]. Briefly final CFU/CFU at 0 h) × 100. The results are presented as the average from 5 independent replicas.

Construction and verification of deletion mutants.

We inactivated the major curli subunit protein gene *csgA* and the colonic acid precursor gene *wza*. Although both pathways involve many genes, the removal of these two components impair the production of both substances respectively. These mutants were generated in *E. coli* K-12 strain MG1655 following the methodology described elsewhere [2] with some modifications because we used as template the genomic DNA of the Keio collection [3]. Briefly, we extracted genomic DNA from the mutants *csgA::Kn* and *wza::Kn* of the Keio collection (*E. coli* BW25113) and amplified by PRC the flanking regions of the kanamycin resistance cassette disrupting both genes and including an appropriate homology sequence. For the *csgA* mutant we used the primers 5'-GATGCCAGTATTTCGCAAGGTG-3' and 5'-GGTTATCTGACTGGAAAGTGCC-3' while primers 5'-TAGCGTGTCTGGATGCCTG-3' and 5'-CCACTTTCAGCTCCGGGT-3' were used for *wza*. The PCR products were purified and electroporated in the *E. coli* MG1655 carrying a red recombinase helper plasmid, pKD46. The strain was grown in 10 ml SOB medium with ampicillin (100 µg/ml) and L-arabinose at 30°C to an OD_{600} of ~0.5 and then made electrocompetent by washing and centrifuge them with a cold solution of glycerol 10%. Competent cells in 80 µl aliquots were electroporated with 200 ng of PCR product. Cells were added immediately 0.9 ml of SOC, incubated during 2 h at 37°C, and then 100 µl aliquots spread onto LB agar with kanamycin (30 µg/ml). The correct inactivation of genes was verified by PCR. The antibiotic resistant cassette (Kn) was removed for both mutants using the flippase plasmid pCP20.

Transcriptome sequencing.

The transcriptome sequencing of primed cells was determined on samples treated identically as described for the priming experiments. Total RNA from 10^8 cell per sample was isolated using the RNAeasy Isolation kit (Qiagen, Germany). Traces of genomic DNA were removed from 10 µg of RNA by digestion in a total volume of 500 µl containing 20 units of TURBO DNase, incubated for 30 minutes at 37°C, immediately followed by RNeasy (Qiagen) clean-up and elution in 30 µl of RNase-free water. Following DNase treatment, RNA integrity was assessed using Agilent RNA 6000 Nano kit and 2100 Bioanalyzer instrument (both from Agilent Technologies). Total RNA was depleted from ribosomal RNA using the Ribo-Zero Depletion Kit for Gram-negative bacteria (Illumina, USA). Libraries were prepared using a TruSeq Stranded Total RNA library preparation kit (Illumina, USA) and were sequenced on a MiSeq platform.

Transcript abundances were derived from pseudo-alignment of reads to the cDNA sequences from the ASM584v2 assembly of *Escherichia coli* MG1655 (ENA accession GCA_000005845.2) using Salmon version 0.7.2 with default parameters [4]. Differential gene expression was analyzed using the R package DESeq2 [5] in conjunction with tximport [6]. Pairwise contrasts were performed between the control and each AMP treatment with empirical bayesian shrinkage of both dispersion parameters and fold-change estimation. We defined genes as being significantly differentially expressed when the absolute fold-change in expression was greater than 2, at an FDR-adjusted p-value of less than 0.05. The variance-stabilizing transformation was used to remove the dependence of the variance on the mean and to transform data to the log2 scale prior to ordination using principal component analysis. Quality of RNAseq data were contrasted by Euclidian distance and symmetry of data reads distribution (Fig. S18).

Observation at single cell level.

To observe cell reaction at single cell level during priming experiments, we used an ad hoc microfluidic device developed for this project. It consisted in a main channel for bacterial inoculation and medium perfusion and with several lateral compartments which dimensions are around 1.5 µm height (ensuring all bacteria are kept in focus) and square 200 µm width corresponding to a field size of the used microscope at 1000x magnification (Fig. SX8). The chip was designed in Autocad (Fig. S19). We started the replication of our microfluidic chips from a

custom made (Sigatec SA) silicon (SiO) master. This silicon master itself was first replicated in Smooth-Cast 310 (Bentley advanced material). Soft lithography produced the chips in PDMS (Sylgard Silicone Elastomer Base and Curing Agent mixed in 10:1 ratio). The PDMS chips were cured overnight at 75°C in an incubator. We punched an inlet and outlet hole for the laminar flow in each chip using a biopsy puncher of 0.5 mm (outer diameter). The chips were bonded to a glass cover slide (24×60 mm) after a 30-second air plasma treatment (PDC-002, Harrick Plasma). Before use, the assembled chip was treated for 15 seconds in air plasma and immediately injected it with filtered MHB medium for passivation. We left the activated chip to incubate for a least 1 hour before loading the bacteria. The devices were loaded to full capacity with a bacterial suspension containing nearly $2x10^8$ CFU/ml (exponentially growing bacteria, 0.5 OD_{600}). Cell suspension was injected into the main channel of the chip using a blunt-end 23G needle attached to a 1ml syringe. We centrifuged the loaded chip at 200 x g for 10 min using in-house adapters, checked the loading.

After we loaded the bacteria cells in the dead end side channels, we connected the chip to a syringe pump (AL-6000, WPI, Germany) and placed the chip under an inverted microscope. A continuous laminar flow (100µl/h) of MHB through the central channel throughout the experiment (SM Fig. 1). For the life cell imaging, after infusion with priming or triggering concentration of AMPs, we injected MHB supplemented with bacterial Live/Dead stain kit solutions (Thermo Scientific, Germany) for a final concentration of 0.1 µl/ml of MHB. We took pictures of at least 20 fields per treatment. Fluorescent images were taken of each field of view with simultaneous acquisition in red and green fluorescent channels during a time interval of no more than 2 minutes per treatment with a Nikon Ti-2 inverted microscope (Nikon, Japan). Cells were observed with the 100× objective and controlled by Nis Element AR software. The chip holder is temperature controlled at 37°C.

Determination of melittin- induced curli.

The production of curli due to melittin treatment was determined by using the fluorescent dye Ectracer^{TM680} (Ebba Biotech, Sweden) that stain extracellular curli. Ectracer^{TM680} was used according to the instructions of manufacturers. Bacterial cultures were treated on chip with priming and triggering concentrations of melittin as described for single cell observation section omitting the live/dead staining. After priming and triggering, the channels were perfused MHB supplemented with Ectracer^{TM680} in a proportion of 1/1000 related to the medium. Cells were observed with the red channel fluorescence for Cy5 dye using a Nikon Eclipse Ti2 inverted optical microscope using the 100X oil objective. Two independent samples were prepared for each group (primed and naïve cells).

SEM of *E. coli* treated antimicrobial peptides.

Approximately $2×10^7$ CFU/ml *E. coli* MG1655 were treated with 1/10 MIC of pexiganan and melittin during 30 minutes. The cultures were concentrated 10 times by a quick centrifugation step of 1 minute at 8 000 g and resuspended in 1/10 of its own supernatant. and resuspension 10 µl drops were placed on a circular glass cover slip (1.5 cm of diameter). The drops were fixed with osmium tetroxide vapors during one minute and allow to dry in a laminar flow cabinet. The cover glasses were mounted on aluminum stubs using double-sided adhesive tape and coated with gold in a sputter coater (SCD-040; Balzers, Union, Liechtenstein). The specimens were examined with a FEI Quanta 200 SEM (FEI Co., Hillsboro, OR) operating at an accelerating voltage of 15 kV

under high vacuum mode at different magnifications. At least 5 fields from two independent replicas.

Statistical analysis.

To analyze the priming data, we first tested if the dynamics of the depicted in the time-kill curves are biphasic.

We fitted the function

$$f(m_1, m_2, t_{kink}, t) = \begin{cases} log_{10}\big(CFU(t=0)\big) + m_1 t, & t < t_{kink} \\ log_{10}\big(CFU(t=0)\big) + m_1 t_{kink} + m_2(t - t_{kink}), & t \geq t_{kink} \end{cases}$$

to the time-kill data of each AMP and for primed and naïve populations individually using RSS.

Here, t_{kink} is the time point, at which the population dynamics switch from the first phase to the second phase and m_1 and m_2 are the slopes of the first and the second decline, respectively.

Note that m_1 is a direct measure of tolerance. The standard error (SE) was calculated as

$$SE(\theta) = \sqrt{\frac{1}{I(\theta)}}$$

Here, θ denotes to the estimated parameter values of m_1, m_2, and t_{kink} and $I(\theta)$ is the expected Fisher information. The 95% CI interval was calculated as $\theta \pm 1.96 * \mathrm{SE}(\theta)$.

Population models.

To describe bacterial population dynamics, we used the two-state model by Balaban *et al.* [7] (Fig. S8):

$$\frac{dN(t)}{dt} = (r_N(A) - s_N)N(t) + s_P P(t)$$
$$\frac{dP(t)}{dt} = (r_P(A) - s_P)P(t) + s_N N(t)$$

In this model, the population $B(t)$ consists of 2 subpopulations $N(t)$ and $P(t)$, with $B(t) = N(t)+P(t)$. The rate of change of the population is determined by the net growth rate of N and P, r_N and r_P, and the switching rate from N to P, s_N, and the switching rate from P to N, s_P. The analytical solution of this ODE system [7,8] is

$$B(t) = N(t) + P(t) = c_1 u_1 e^{\lambda_1 t} + c_1 u_2 e^{\lambda_1 t} + c_2 v_1 e^{\lambda_2 t} + c_2 v_2 e^{\lambda_2 t} \quad \text{Eq. S2}$$

with

$$\lambda_1 = \frac{r_N + r_P - s_N - s_P - \sqrt{(-r_N - r_P + s_N + s_P)^2 - 4(r_N r_P - r_P s_N - r_N s_P)}}{2}$$

$$\lambda_2 = \frac{r_N + r_P - s_N - s_P + \sqrt{(-r_N - r_P + s_N + s_P)^2 - 4(r_N r_P - r_P s_N - r_N s_P)}}{2}$$

$$\vec{u} = \begin{pmatrix} \frac{\lambda_1 - r_P + s_P}{s_N} \\ 1 \end{pmatrix}$$

$$\vec{v} = \begin{pmatrix} \frac{\lambda_2 - r_P + s_P}{s_N} \\ 1 \end{pmatrix}$$

$$c_1 = \frac{v_1 P(t=0) - N(t=0)}{v_1 - u_1}$$

$$c_2 = \frac{-u_1 P(t=0) + N(t=0)}{v_1 - u_1}$$

The model was fitted by minimizing the RSS, similar to the above. For the starting conditions ($N(t=0)$, $P(t=0)$, we assumed that the ratio of N/P was constant over time when the exposure to lethal concentrations of AMPs started. $N(t=0)$ and $P(t=0)$ were therefore calculated using the eigenvector $\vec{v}$ that corresponds to the largest eigenvalue of a system without antimicrobials. Here, we assumed that the parameter r_N is equal the net growth rate in absence of antimicrobials, $r_N = \psi_{max}$. The parameter ψ_{max} was estimated based on the time-kill curve of bacterial population that grow in absence of antimicrobials (see below). The eigenvector contains information about the ratio of N and P for $t \to \infty$: $\frac{N}{P} = \frac{v_1}{v_2}$. Resulting, $P(t=0) = \frac{B(t=0)}{1+v_1}$ and $N(t=0) = B(t=0) - P(t=0)$. $B(t=0)$ was estimated from the data. Confidence intervals were calculated as described above. In a pre-analysis, we used 4 free model parameters that were fitted: r_N, r_P, s_N and s_P. The parameter r_P was not significant from (Fig. S4). Therefore, we set the parameter r_P to 0 and fitted the remaining 3 parameters to the data (table S6).

Tolerance and persistence in terms of model parameters

The measure of tolerance is the slope m_1. Komarova and Wodarz [8] showed that the slope can directly be linked to the population model parameters. In our notation,

$$m_1 = log_{10}\left(c_1(u_1+v_1)e^{\lambda_1 t}\right) \text{ Eq. S1}$$

Note that the first phase is mainly influenced by r_N (Fig. S9), therefore, $m_1 \approx r_N$.

Persistent cell numbers at time t were calculated with the analytic solution:

$$P(t) = c_1 u_2 e^{\lambda_1 t} + c_2 v_2 e^{\lambda_2 t} \text{ Eq. S2}$$

Pharmacokinetic and pharmacodynamic function.

We used the pharmacokinetic function $A(t) = A_{max} e^{-k(t-n)}$, with $8h * n \leq t \leq 8h * (n+1)$ and $n = 0,1,2 \ldots$ described previously elsewhere [9]. In our simulations, we fixed the decay parameter k and varied the drug input A_{max}. To describe the effect of the AMPs on the bacterial population, we used the pharmacodynamic (PD) function $\psi(A)$ [9,10], with

$$\psi(A) = \psi_{max} - e(A) = \psi_{max} - \frac{(\psi_{max} - \psi_{min})\left(\frac{A}{MIC}\right)^{\kappa}}{\left(\frac{A}{MIC}\right)^{\kappa} - \frac{\psi_{min}}{\psi_{max}}}$$

The parameter ψ_{max} describes the net growth rate in absence of antimicrobials ($\psi_{max} = \psi(A = 0)$). The antimicrobial effect $e(A)$ is dependent on the antimicrobial concentration and is the defined with ψ_{max}, ψ_{min}, the net growth rate in presence of large amounts of antimicrobials ($\psi(A \to \infty)$), with the MIC, the antimicrobial concentration that results in no growth ($\psi(A = MIC) = 0$) and with κ, which determines the steepness of the PD curve.

The PD function was fitted to the time-kill curves (Fig. S6), as described by Regoes *et al.* [9]. In short, we used log-linear regressions of the time kill curves within the time-points 0h and 1h to estimate the change of the bacterial population over time, i.e. the slopes of the log-linear regression. We fixed the parameter ψ_{max} and fitted the 3 remaining parameters of the PD function with the *Markov-Chain-Monte-Carlo method.*

Stochastic simulations.

To simulate resistance evolution with stochastic simulations, we expanded a previously developed framework for bacterial population dynamics [11]. The framework models bacterial population dynamics exposed to changing levels of antimicrobials and allows for resistance evolution. In the simulations, the change in population size of a sensitive strain *S*, with *S* = *N*+*P*, and of a resistant strain *R* were described with the following ODE system:

$$\frac{dN(t)}{dt} = \psi_{max}(1-\mu)N(t)\left(1-\frac{N(t)+P(t)+R(t)}{K}\right) - s_N N(t) + s_P P(t) - e_N(A(t))N(t)$$

$$\frac{dP(t)}{dt} = s_N N(t) - s_P P(t)$$

$$\frac{dR(t)}{dt} = \psi_{max}\,\mu\, N(t)\left(1-\frac{N(t)+P(t)+R(t)}{K}\right) + \psi_{max}(1-c)R\left(1-\frac{N(t)+P(t)+R(t)}{K}\right) - e_R(A(t))R(t)$$

Here, the replication rate is assumed to be equal to the maximum net growth rate ψ_{max}. The effect of the antimicrobial $e_N(A)$ is explained above. Note that we assume that bacteria in class P do not grow and are not affected by antimicrobials. We also assumed that the switching rates are constant. To describe the effect of an antimicrobial on the strain *R*, $e_R(A)$, we use the same parameter set than with $e_N(A)$, except for the *MIC*: $\frac{MIC_R}{MIC_N} = 10$. In the simulations, we differentiated between the following cases: (i) naïve bacteria, homogeneous population (no persistence), (ii) naïve bacteria, heterogeneous population, (iii) primed bacteria (increase in r_N), homogeneous population, (iv) primed bacteria (increase in r_N), heterogeneous population (v) primed bacteria (increase in r_N and decrease in s_P). The stochastic simulations were run 1000 times for each antimicrobial, for each case, and for a variety of input antimicrobial concentrations A_{max}. All parameter values are listed in table S7. The intensity is the input antimicrobial concentrations A_{max}. The simulations were run for t=7d. Time until clearance and probability of resistance evolution were calculated as the mean of the value over the 1000 simulations.

Implementation

Statistical testing, simulations and plots were done in R version 3.3.2 [12], using Rstudio version 1.0.143 [13]. We used the following R-packages: (i) for plotting: sfsmisc [14], (ii) for fitting

the PD function: rjags(iii) for stochastic simulations: adaptivetau [15]. We used Mathematica version 11.0 [16] to determine the analytical solutions of the population models.

Figures

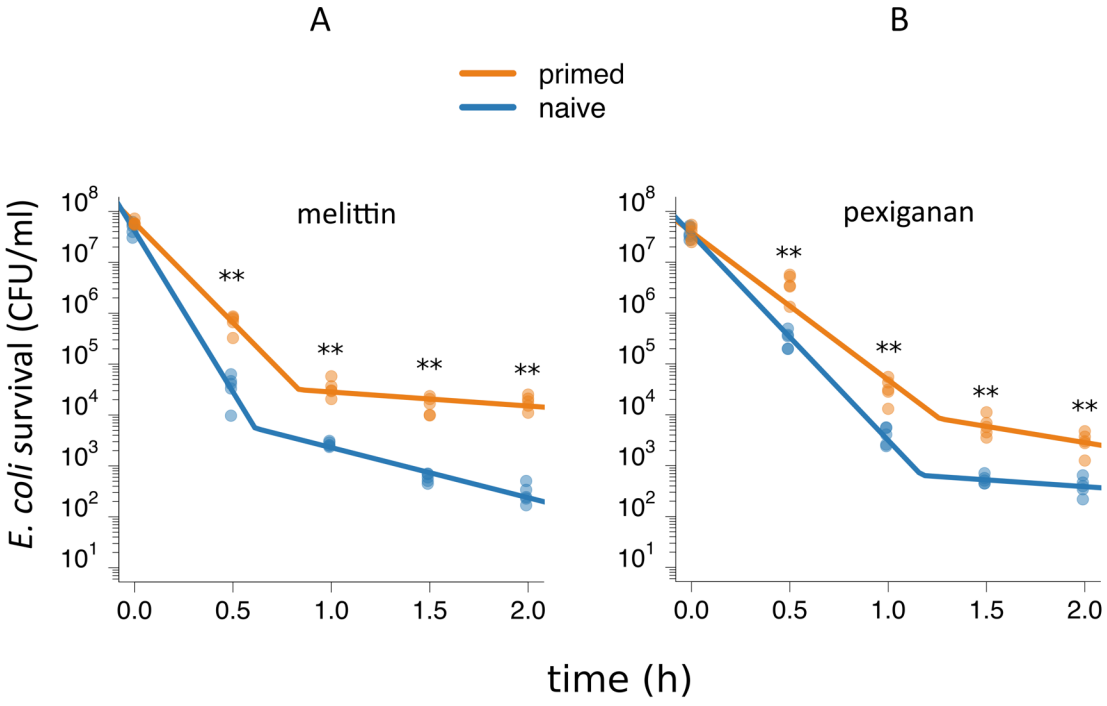

Fig. 1: Bacterial tolerance and persistence determine the shape of time-kill curves. Time-kill experiments with *E. coli* K-12, naïve (blue) and primed (orange) bacteria were exposed to 10xMIC of (A) melittin and (B) pexiganan. In both cases priming significantly increased the slope in the first phase (tolerance, $p<0.05$) and the bacterial count in the second phase (persistence, $p<0.05$). The line in the plots indicates the best fit of a biphasic function (table S3).

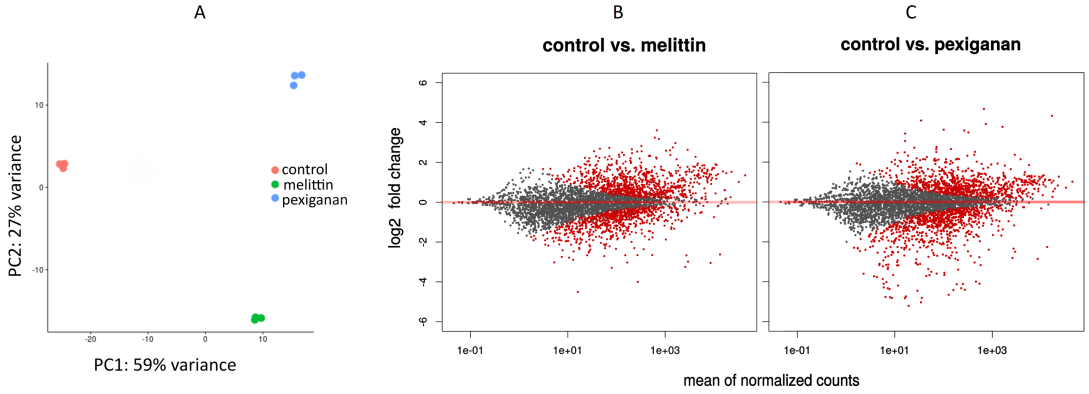

Fig. 2. Gene expression in primed *E. coli*. (A) Principal component 1 separates the control from the peptide priming, PC 2 separates the melittin induced response from the pexiganan response. (B) Global expression patterns of cells primed with 0.1 MIC melittin and (C) pexiganan (Fig. S3, S4, S5, S18).

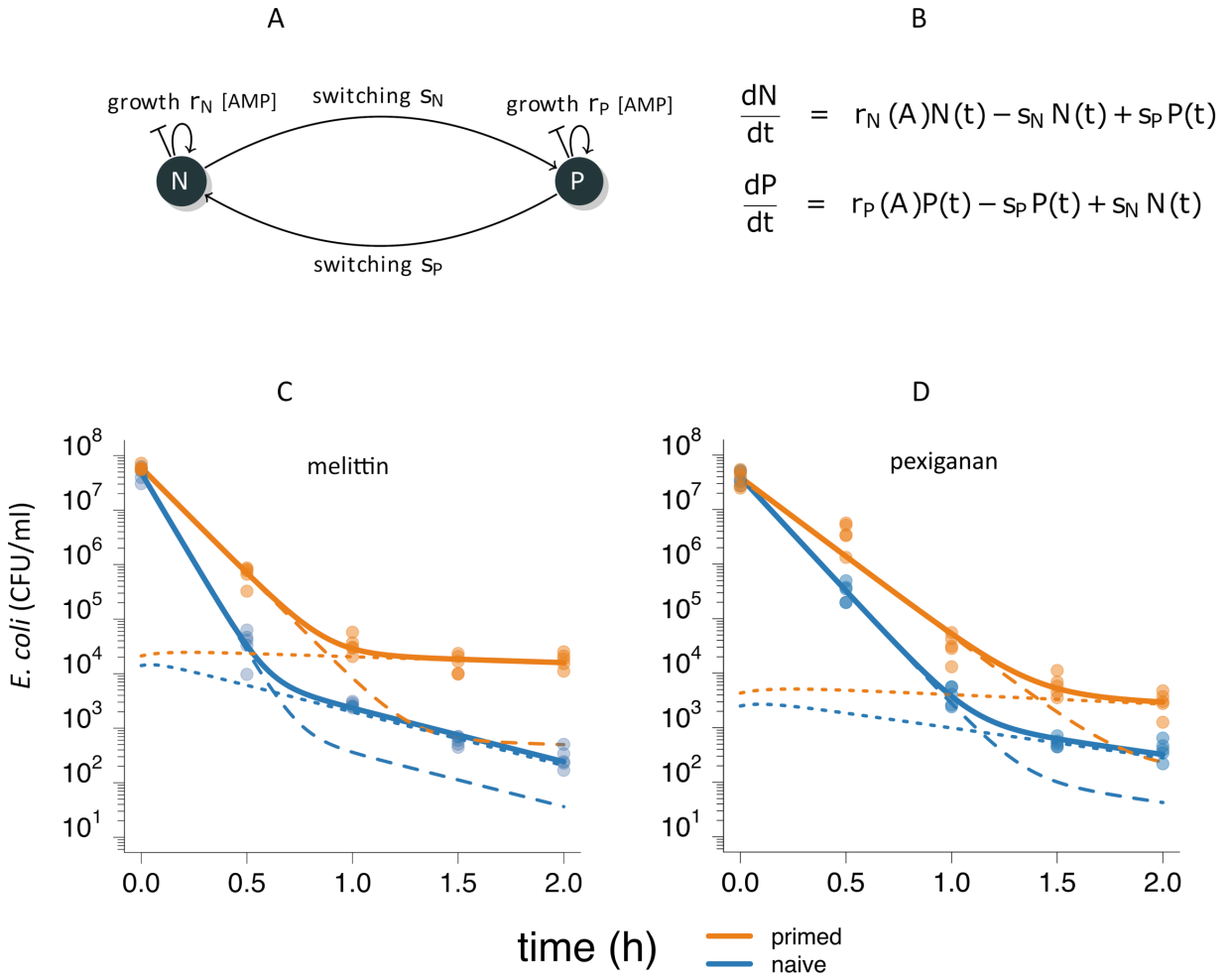

Fig. 3: The two-state model (A, B, adapted from *11*) describes time-kill data and fits the empirical data well (parameters: main text). We fitted the time-kill data of bacteria exposed to melittin (C) and pexiganan (D) (naïve, blue; primed orange). Bacteria primed with melittin have an increased net growth rate r_N and decreased s_P compared to the naive populations. For pexiganan, the parameter r_N is significantly higher in primed compared to naïve populations (all fitted parameters in figure S11, S12) The resulting population model mimics the data well. The continuous line represents the total bacterial population B(t) and the dashed and dotted lines represent the subpopulations N(t) and P(t).

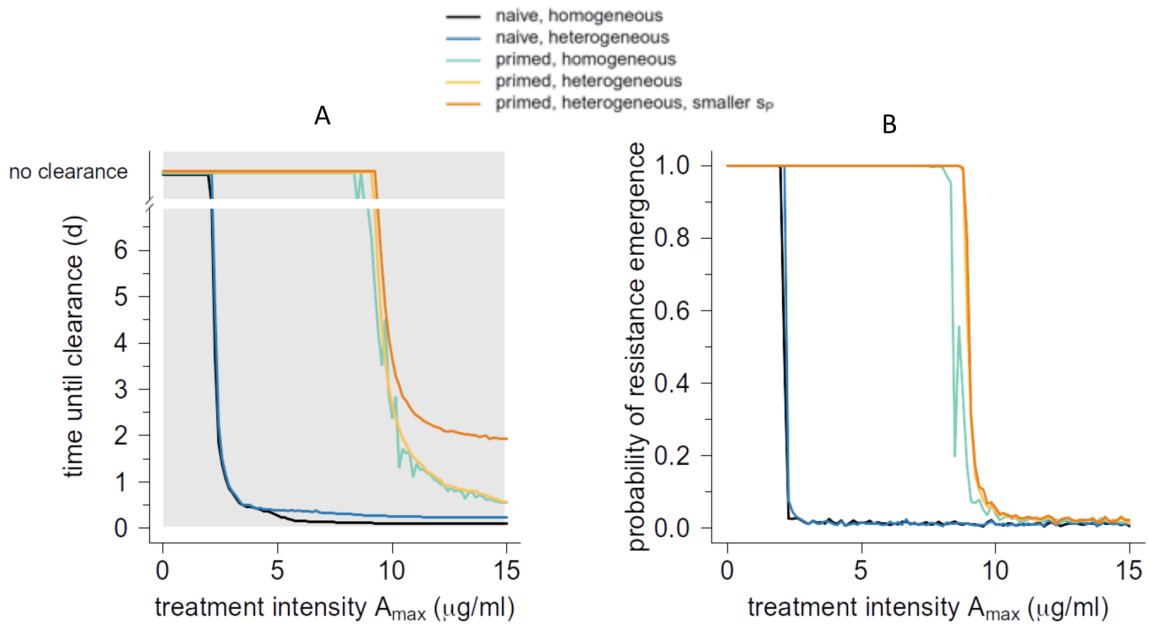

Fig. 4: Influence of priming on time until clearance and resistance evolution. We extended a previously developed PKPD framework (*7*) to include persistence (Fig. S2B). With this framework, we estimated PD curves (Fig. S14) for primed and naïve bacteria and the estimated switching rates (Fig. 3) to predict (A) time until clearance and (B) probability of resistance evolution. We simulated the two cases of primed (primed, heterogeneous, smaller *sP*) and naïve bacteria (naïve, heterogeneous). In addition, we simulated homogeneous naïve and primed populations and primed population with switching rates of the naïve population. No clearance means that simulated treatment could not reduce bacteria population < 1 cell. Here, we only show the results of melittin (results of pexiganan are qualitatively highly similar, see Fig. S15). All parameter values used are listed in Table S7. *rN* and decreased *sP* compared to the naive populations. Here, the continuous line represents the total bacterial population *B(t)* and the dashed and dotted lines represent the subpopulations *N(t)* and *P(t),* respectively.

Supplementary tables

Table **S** 1. Minimal inhibitory concentration of the two antimicrobial peptides melittin and pexiganan and the antibiotic ciprofloxacin used in this work. The MIC was determined to be used as a concentration reference but it was also determined after priming treatment to show that the observed enhanced survival is based on a phenotypic changes and not mutations.

Antimicrobials	MIC (µg/ml) pre-priming	MIC (µg/ml) post-priming
melittin	2	2
pexiganan	1	1
ciprofloxacin	0.125	0.125

Table S 2. Test for significant differences between naïve and primed bacteria at each time point t and for each antimicrobial. Significance was tested with the Mann–Whitney–Wilcoxon test (n_1 = n_2 = 5 at each time point, $p < 0.05$). P-values (rounded values are presented here) were adjusted for multiple testing. Significant differences between primed and naïve population counts are indicated with asterisks at each time point and for each antimicrobial.

$t(h)^{\S}$	*p*-value			
	melittin		pexiganan	
0	0.151		1	
0.5/1	0.040	*	0.040	*
1/2	0.040	*	0.040	*
1.5/3	0.040	*	0.040	*
2/4	0.040	*	0.040	*

§ time-point AMP/AB

Table S 3. Slopes of fitting a biphasic function with the slopes m_1 and m_2 to the data. Note that the values are rounded and that significant differences between slopes of primed and naïve population counts are indicated with asterisks for each antimicrobial.

Antimicrobial	Treatment	Slope			
		m_1 (± SE)		m_2 (± SE)	
melittin	Primed	-3.925 (0.632)	*	-0.275 (0.447)	
	Naïve	-6.330 (0.632)		-0.984 (0.447)	
pexiganan	Primed	-2.906 (0.283)	*	-0.635 (0.894)	
	Naïve	-4.055 (0.283)		-0.266 (0.894)	

Table S 6. Results of fitting the two-state model to bacterial population dynamics in the presence of melittin and pexiganan and the classic exponential population growth model to dynamics in the presence of ciprofloxacin and ampicillin (rounded values).

Antimicrobial	Treatment	r_N (± SE)	r_P[1]	s_N (± SE)	s_P (± SE)
melittin	Primed	-8.960 (0.717)	0	0.00085 (0.00098)	0.27 (0.61)
	Naïve	-15.061 (0.858)	0	0.00128 (0.00095)	2.25 (0.45)
pexiganan	Primed	6.681 (0.319)	0	0.00027 (0.00059)	0.40 (1.10)
	Naïve	-9.610 (0.400)	0	0.00021 (0.00025)	1.26 (0.66)

[1] Parameter r_P is fixed at 0 due to results of a preliminary analysis.

Extended data table 7. Parameter values used in the stochastic simulations.

Parameter	Description	AMP	Value
k	AMP degradation rate		0.5
μ	Mutation rate		$1*10^{-9}$
K	Carrying capacity		$5*10^{9}$
ψ_{max}	Maximal net growth rate in absence of antimicrobials	melittin	2.13
		pexiganan	2.06
ψ_{min}	Minimal net growth rate in presence of large amounts of antimicrobials	melittin	-8.86/ -9.89[§]
		pexiganan	-36.87/-66.80[§]
κ	Hill parameter	melittin	1.3/1.1[§]
		pexiganan	0.6/0.7[§]
MIC	Dose of antimicrobials for which the net growth rate is 0	melittin	0.48/1.83[§]
		pexiganan	0.54/2.14[§]
c	Cost of resistance		0.5
$B(t=0)$	Population size at time t=0		10^{8}
t_{max}	Maximal run of simulation		7d
s_N	Switching rate from N to P	melittin	0.0012
		pexiganan	0.00021
s_P	Switching rate from P to N	melittin	2.26/0.28[§]
		pexiganan	1.26/0.40[§]

§ **Naïve/Primed**

Supplementary table 4 (separate excel file). Priming response to melittin (0.1xMIC, 30-minute treatment)

Supplementary data table 5 (separate excel file). Priming response to pexiganan (0.1xMIC, 30-minute treatment)

Supplementary References

1. Patro R, Duggal G, Love MI, Irizarry RA, Kingsford C. Salmon provides fast and bias-aware quantification of transcript expression. Nat Methods [Internet]. Nature Publishing Group; 2017 [cited 2019 Jul 3];14:417–9.

2. Love MI, Huber W, Anders S. Moderated estimation of fold change and dispersion for RNA-seq data with DESeq2. Genome Biol [Internet]. 2014 [cited 2019 Jul 3];15:550.

3. Soneson C, Love MI, Robinson MD. Differential analyses for RNA-seq: transcript-level estimates improve gene-level inferences. F1000Research [Internet]. 2015 [cited 2019 Jul 3];4:1521.

4. Balaban NQ, Merrin J, Chait R, Kowalik L, Leibler S. Bacterial Persistence as a Phenotypic Switch. Science (80-) [Internet]. 2004 [cited 2018 Jun 9];305:1622–5.

5. Komarova NL, Wodarz D. Effect of Cellular Quiescence on the Success of Targeted CML Therapy. Agur Z, editor. PLoS One [Internet]. 2007 [cited 2018 Jun 9];2:e990.

6. Regoes RR, Wiuff C, Zappala RM, Garner KN, Baquero F, Levin BR. Pharmacodynamic Functions: a Multiparameter Approach to the Design of Antibiotic Treatment Regimens. Antimicrob Agents Chemother [Internet]. American Society for Microbiology (ASM); 2004 [cited 2019 May 30];48:3670. Available from: http://www.ncbi.nlm.nih.gov/pubmed/15388418

7. Yu G, Baeder D, Regoes R, Rolff J. Predicting Drug Resistance Evolution: Antimicrobial Peptides Vs. Antibiotics. Proc R Soc Lond B. 2018;138107.

8. R Core Team. R: A language and environment for statistical computing. Vienna, Austria: R Foundation for Statistical Computing; 2015.

9. R Development Core Team. RStudio Team (2015). RStudio: Integrated Development for R. [Internet]. Boston: MA URL http://www.rstudio.com/; 2015. Available from: http://www.rstudio.com

10. Maechler M. Utilities from "Seminar fuer Statistik" ETH Zurich [R package sfsmisc version 1.1-4]. Comprehensive R Archive Network (CRAN); [cited 2019 Jul 3]; Available from: https://cran.r-project.org/web/packages/sfsmisc/index.html

11. Cao Y, Gillespie DT, Petzold LR. Adaptive explicit-implicit tau-leaping method with automatic tau selection. J Chem Phys [Internet]. 2007 [cited 2019 Jul 3];126:224101. Available from: http://aip.scitation.org/doi/10.1063/1.2745299

12. Wolfram Research I. Mathematica, Version 11.0. Champaign, Illinois: Wolfram Research, Inc.; 2016.

13. Wiuff C, Zappala RM, Regoes RR, Garner KN, Baquero F, Levin BR. Phenotypic tolerance: antibiotic enrichment of noninherited resistance in bacterial populations. Antimicrob Agents Chemother [Internet]. 2005 [cited 2016 Jan 6];49:1483–94. Available from: http://www.pubmedcentral.nih.gov/articlerender.fcgi?artid=1068602&tool=pmcentrez&rendertype=abstract

14. Nielsen EI, Friberg LE. Pharmacokinetic-Pharmacodynamic Modeling of Antibacterial Drugs. Pharmacol Rev [Internet]. 2013 [cited 2019 Jul 4];65:1053–90. Available from: http://www.ncbi.nlm.nih.gov/pubmed/23803529

Supplementary Figures

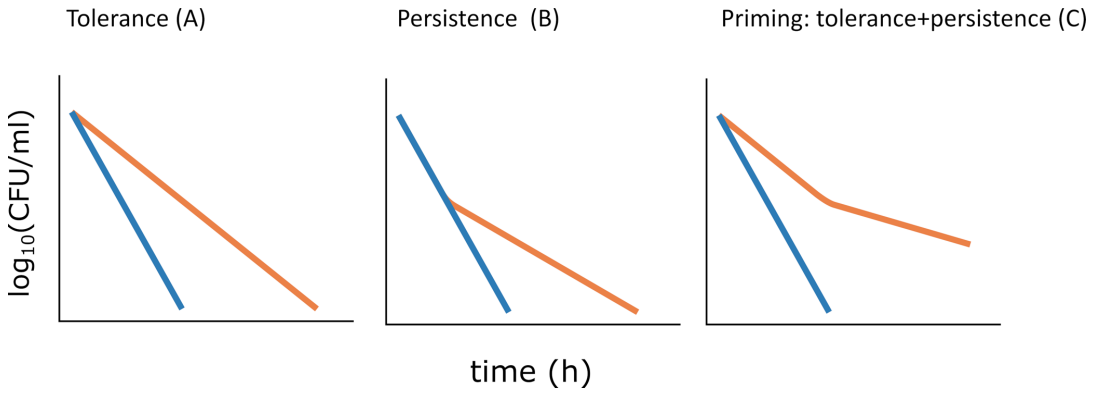

Figure S 1. Bacterial tolerance and persistence change the shape of time-kill curves (figure adapted from Brauner et al. [17]. (A) Tolerance is the ability of bacteria to longer survive exposure to antimicrobials due to decrease in susceptibility. Tolerance is quantified as increase in the slope of the time kill curve. (B) Persistence is the phenomenon of a subpopulation being less susceptible to the antimicrobial than the rest of the population. A persistent subpopulation manifests as a biphasic decline of bacterial population when exposed to lethal concentrations of antimicrobials. Here, the population consists predominantly of the less susceptible persistent subpopulation. (C) Together, tolerance and persistence result in biphasic time-kill curves with decreased susceptibility in the first phase.

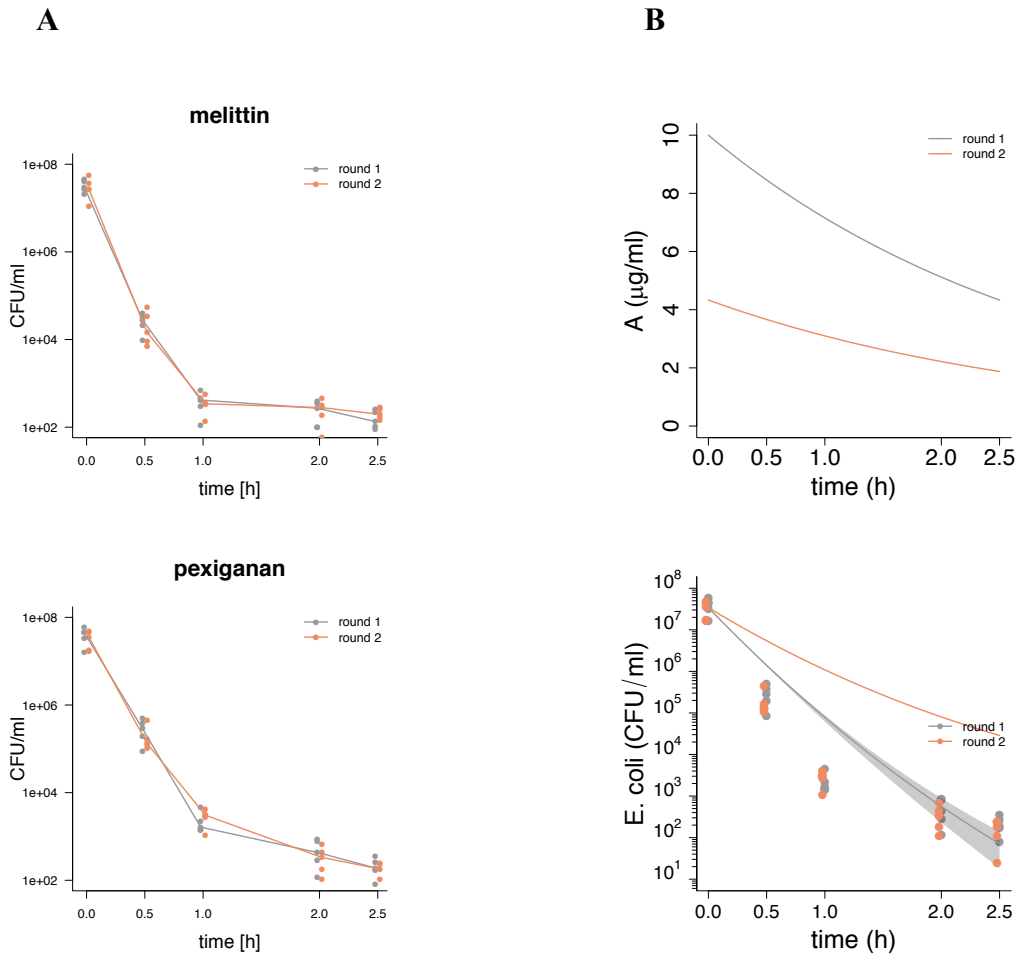

Figure S 2. Bacteria exposed to the AMPs melittin and pexiganan showed a nonlinear decline. We used the two-state model [7] to describe population dynamics. The two-state model assumes a heterogeneous population with respect to phenotypic resistance to the antimicrobial. Due to the heterogeneity in response, the time-kill dynamics are biphasic for lethal doses of the antimicrobial. Another explanation for a nonlinear decline in populations the decrease in active AMP concentration over time due to degradation [18,19], We tested this alternative explanation. (A) As in Fig. 1, we measured the population dynamics of bacteria exposed to 10 x MIC (round 1). At the end of the experiment, we sampled the supernatant. In round 2, a fresh bacterial population was exposed to the sampled supernatant. The trend line is the median of the population size at each time-point. (B) To model the population dynamics assuming decrease in antimicrobial concentration, we used the population model by Wiuff *et al.* [18], which includes the pharmacodynamic function $\boldsymbol{\psi}(\boldsymbol{A})$. The pharmacokinetic function *A(t)* was used to estimate the degradation parameter *k*. For this, we set *A(t = 0)* to 10 x MIC and estimated the antimicrobial decay rate *k* using the time-kill data of the first round. Here we show the results of time-kill experiments with melittin, in the upper plot the pharmacokinetic function and in the lower plot modeling results on top of the experimental data as seen in (A). The line indicates the population dynamics of the model for round 1 and round 2 with the decay rate resulted from the best fit. The

grey area shows the confidence interval of the population dynamics, which was calculated by repeatedly bootstrapping the time-kill data of round 1 when estimating *k*. We then also plotted the population dynamics of the second round. With this analysis, we were able to exclude the decrease in active antimicrobial concentration as explanation of non-linear decrease of bacteria.

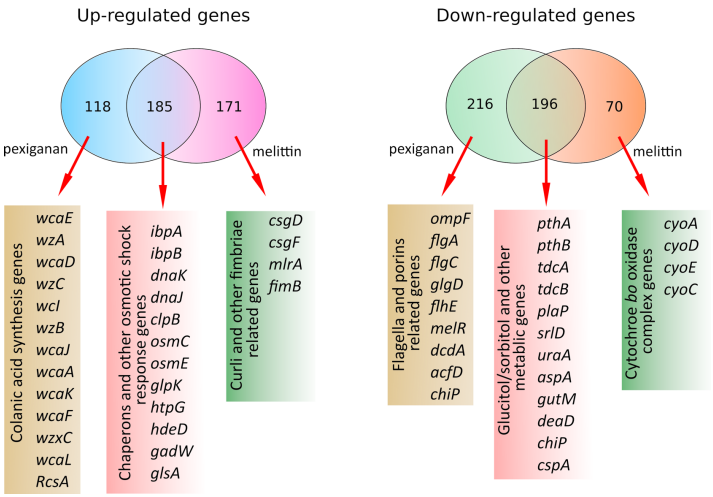

Figure S 3. Venn diagrams showing specific and overlapping responses of *E. coli* MG1655 to priming concentrations of melittin and pexiganan. Selected genes and pathways are indicated to gain clarity on the global response.

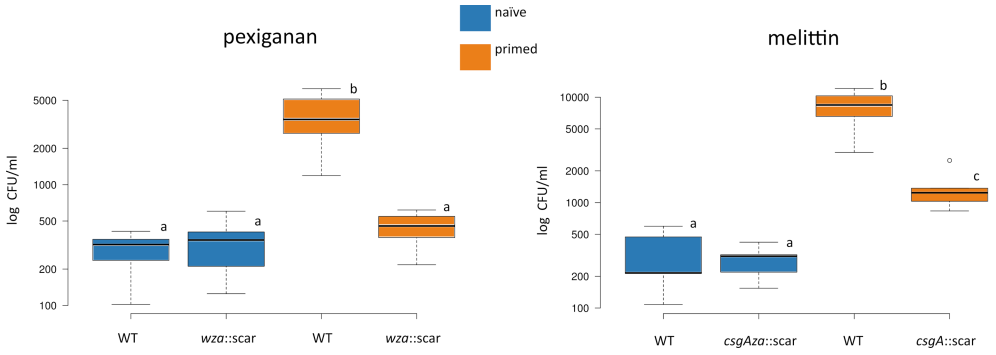

Figure S 4. Bacterial mutants in *csgA* (curli mutant) and *wza* (colonic acid mutant) were exposed to the AMPs melittin and pexiganan respectively (10xMIC) after priming. Colony forming units (CFU) were determined after two hours of exposure. Boxplot show data tested by repeated-

measures of one-way ANOVA and Dunnetts' tests. For each case, equal letter represents no statistical differences while differing letter detonates significant ones (for $p<0.05$).

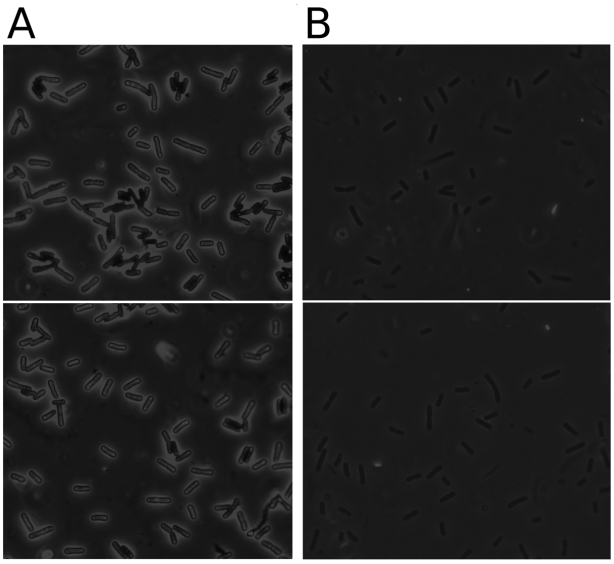

Figure S 5. *E. coli* MG1655 treated with 1/10xMIC (priming concentration) of pexiganan (A) and non-treated bacteria (B, control) observed under phase contrast optical microscopy. The specimens

consisted of cells suspended in a 0.1 % solution of nigrosin to create a strong contract to visualize the colonic acid capsules. Bacteria were observed with magnifications 1000X.

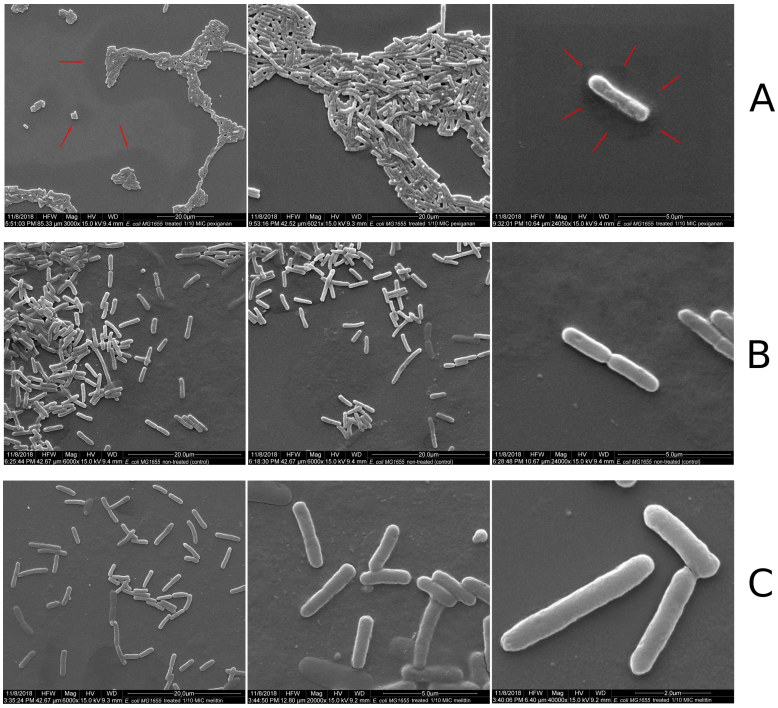

Figure S 6. SEM of E. coli MG1655 treated with 1/10xMIC (priming concentration) of pexiganan (A) and melittin (C) and non-treated bacteria (B, control). No apparent difference was noticed between melittin-treated cells and control. In the case of pexiganan, the treated cells tend to aggregate, a phenotype that consistent with the presence of colanic acid. Red arrows represent potential areas altered by the capsule of colanic acid that collapse under drying processing necessary for the preparation. Bacteria were observed with different magnifications ranging from 3000X to 40000X.

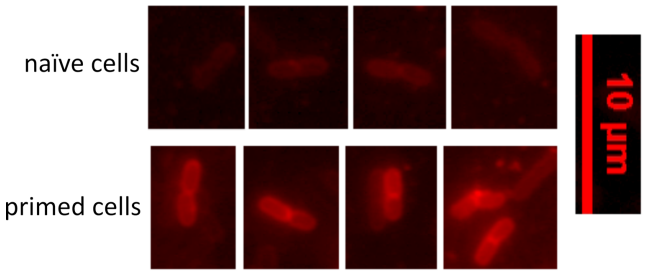

Figure S 7. Detection of curli production by primed cells after exposure to a killing dose of melittin (10xMIC). Curli production is only detected in small proportion of primed cells (survival fraction) after exposure to a trigger stimulus. In this case, after treatment, we exposed the cells to ECtracer™680 (Ebba Biotech, Sweden), a red fluorescent tracer molecule for staining of curli in the bacterial extracellular compartment. In the top panel naïve cells show a discrete autofluorescence allowing to distinguish them from the background in contrast to the lower panel

which strong cumulative red fluorescence on primed cell surface revealing the presence of curli proteins.

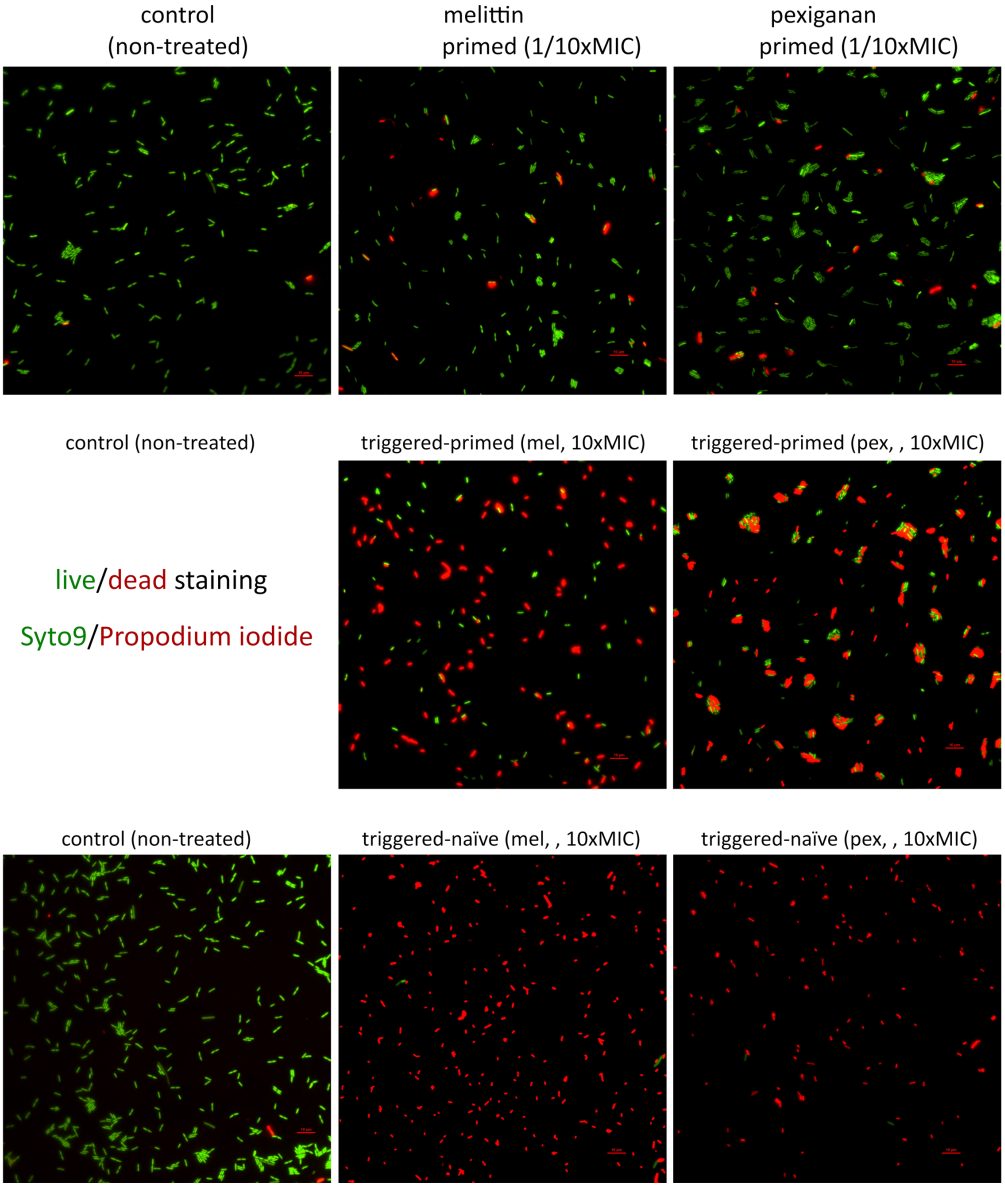

Figure S 8. Cell viability after treating with priming and trigger doses of melittin and pexiganan were determined using the using the live/dead BacLight Bacterial Viability Kit (Thermo Scientific, Germany) on chip as described in M&M. After priming during 30 minutes, the treatment was removed by perfusing fresh MHB. The fluorescence signal was analyzed via a using excitation at

485 nm and emission at 530 nm for green fluorescence (Syto9) and using excitation at 485 nm and emission at 630 nm for red fluorescence (propidium iodide).

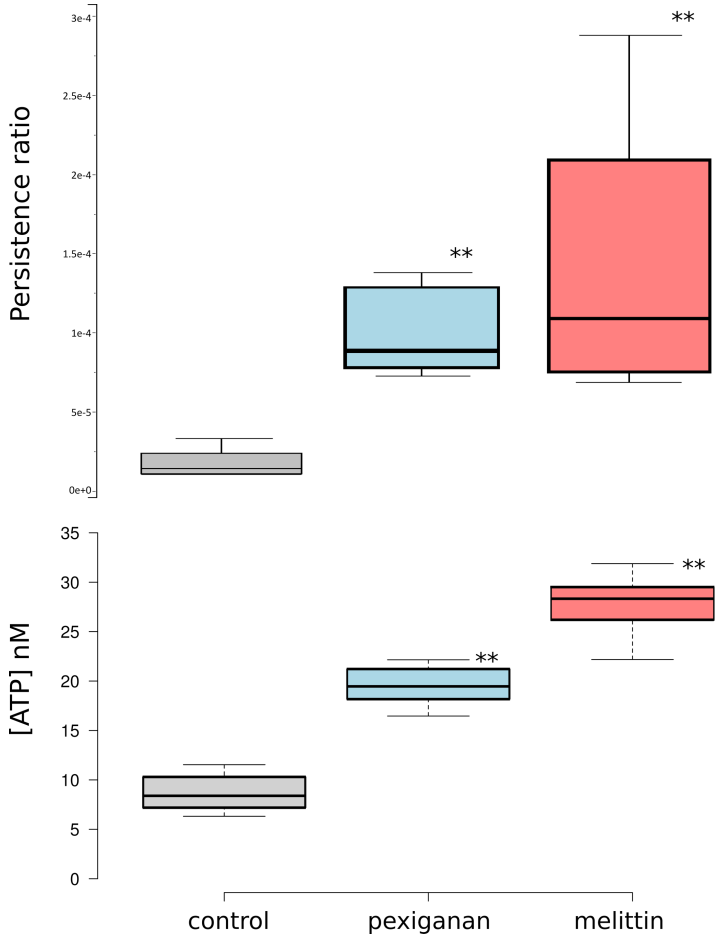

Figure S 9. Priming concentration of pexiganan and melittin increased the persister number as determined by treated primed and naïve populations (10^8 CFU/ml) with ciprofloxacin (2µg/ml). This increase in persistence co-occurs with ATP leakage (determined in the supernatant of culture medium).

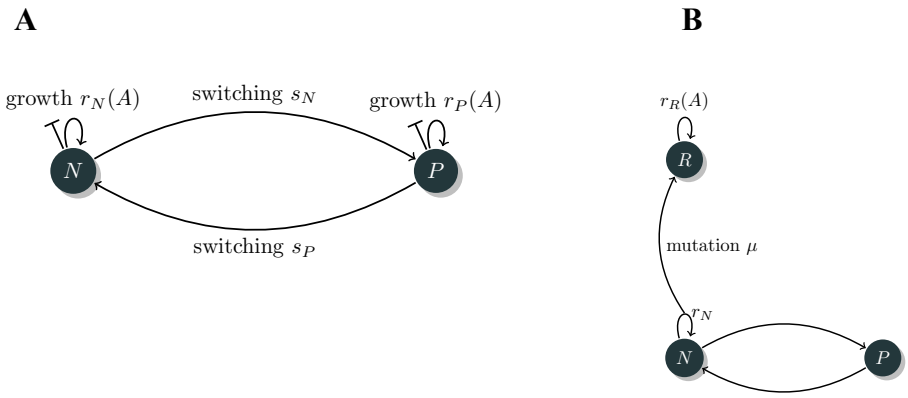

Figure S 10. Diagrammatic representation of (A) the two-state model [7] and (B) our previously developed framework [11], which we extended by a persistent class.

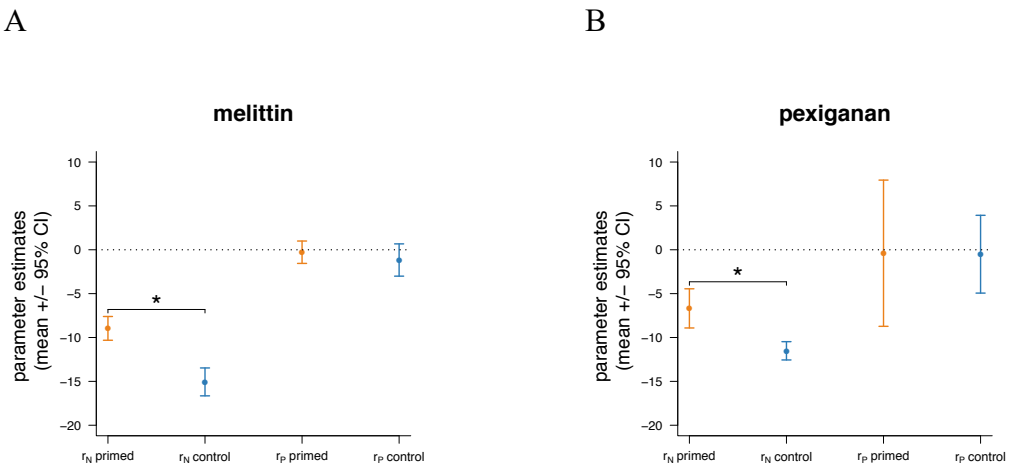

Figure S 11. Net growth rates resulting from the fit of the two-state model with 4 free parameters. For both (A) melittin and (B) pexiganan, r_P is not significantly different from 0. Significant differences between naive and primed treatment are indicated with asterisks.

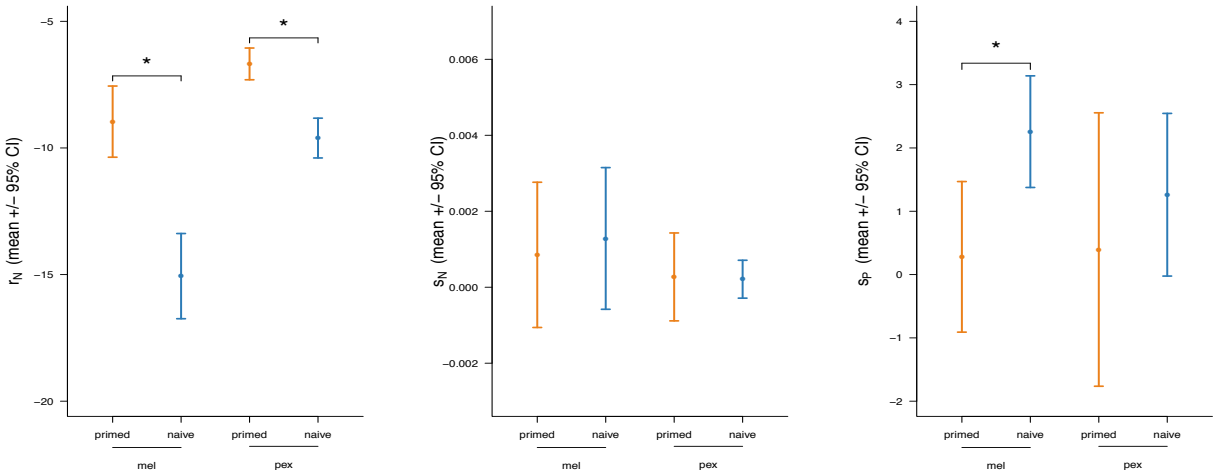

Figure S 12. Parameter values of the two-state model fitted to the data of primed (orange) and naïve (blue) bacteria. The parameter r_P was set to 0. Significant differences between naïve (blue) and primed (orange) parameter values are indicated with asterisks.

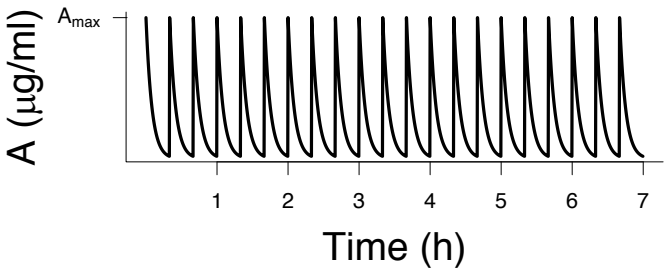

Figure S 13. Pharmacokinetic profile used in our stochastic simulations.

A

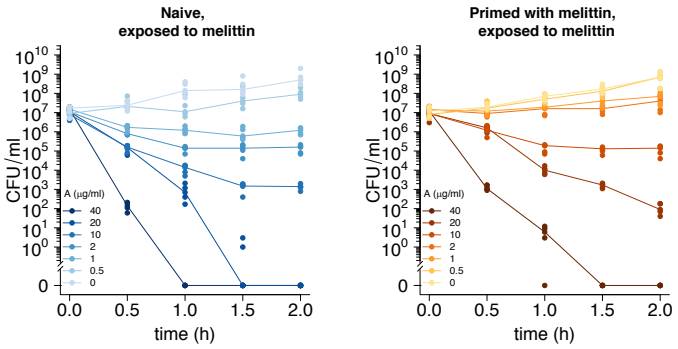

B

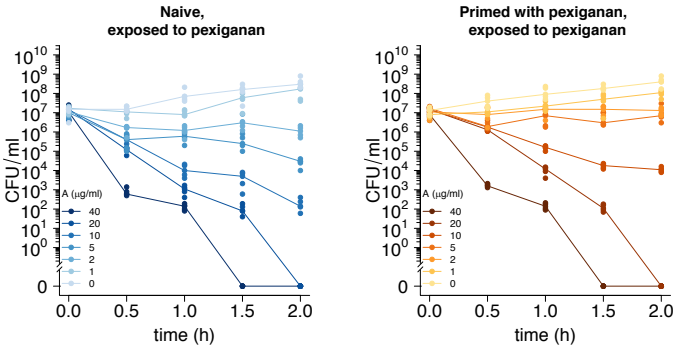

C

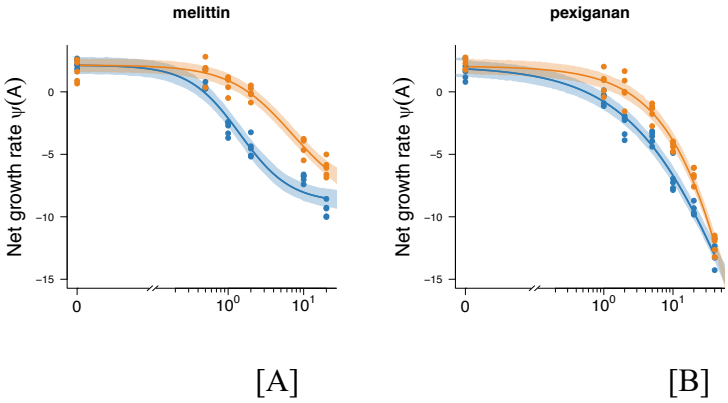

Figure S 14. Time-kill curves and PD curves of bacterial population dynamics exposed to AMPs. Time-kill experiments in which naïve (blue) and primed (orange) bacteria were exposed to (A)

melittin and (B) pexiganan. The AMP dose used in each time-kill experiment is listed in the legend in each plot. (C) PD function fitted to the data in [A] and [B]. Note that we excluded data points of experiments in which naïve bacteria were exposed to melittin (40 µg/ml) from the analysis to ensure the best fit. Parameter values are listed in table S7.

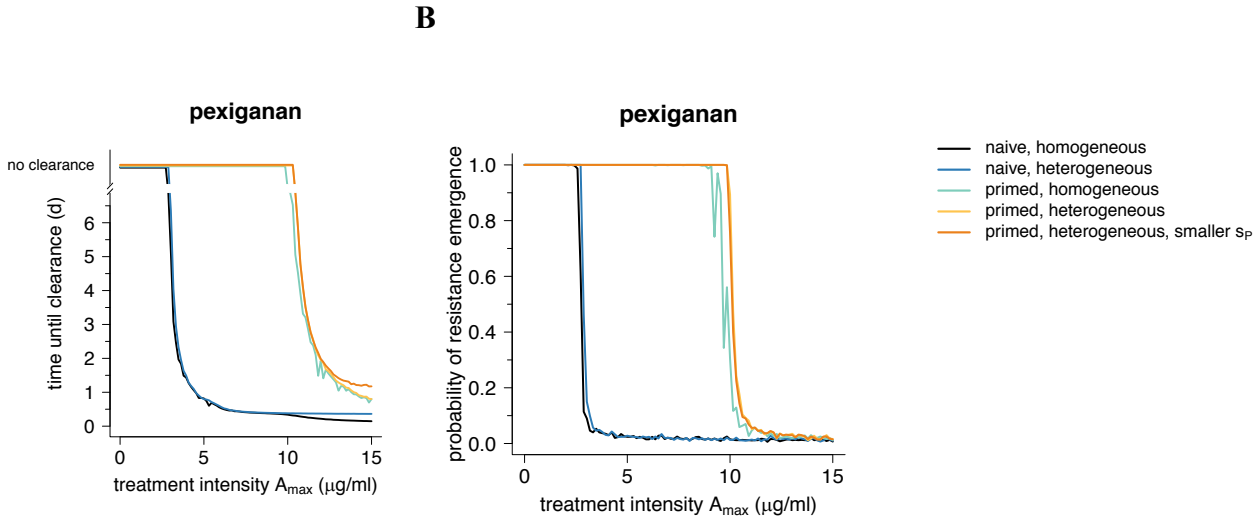

Figure S 15. Time until clearance and probability of resistance evolution for bacteria exposed to pexiganan.

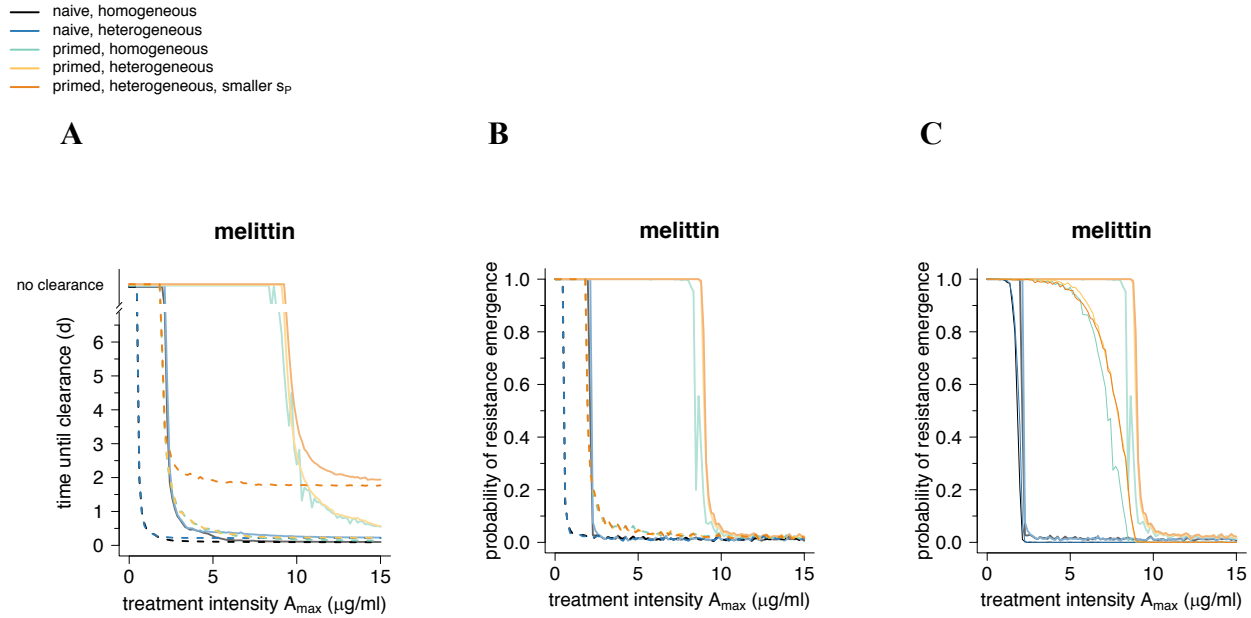

Figure S 16. Predictions for different parameter values. (A) Time until clearance and (B) probability of resistance evolution is affected by the AMP decay rate k (dashed lines: k=0, solid lines: k=0.5). (C) Decreasing the mutation rate (solid lines: $\boldsymbol{\mu = 10^{-9}}$, thin solid line $\boldsymbol{\mu = 10^{-11}}$) decreases the probability of resistance emergence. All other parameter values according to table S7.

A B

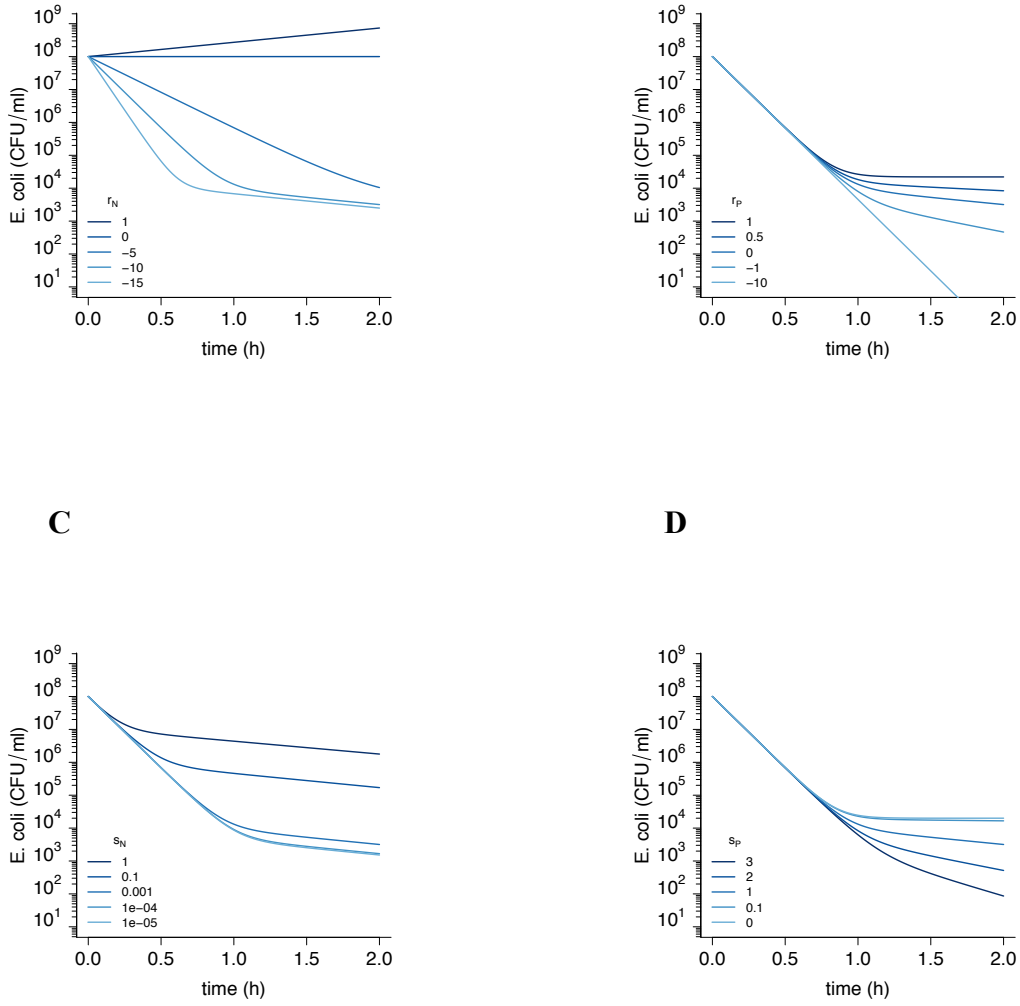

Figure S 17. Two-state model predicts biphasic decline depending on the model parameter values. If not varied, r_N = -10, r_P = 0, s_N = 0.001, and s_P = 1. Tolerance, i.e. the slope m_1 is mainly influenced by r_N, while the levels of persistence is influenced by all four parameters.

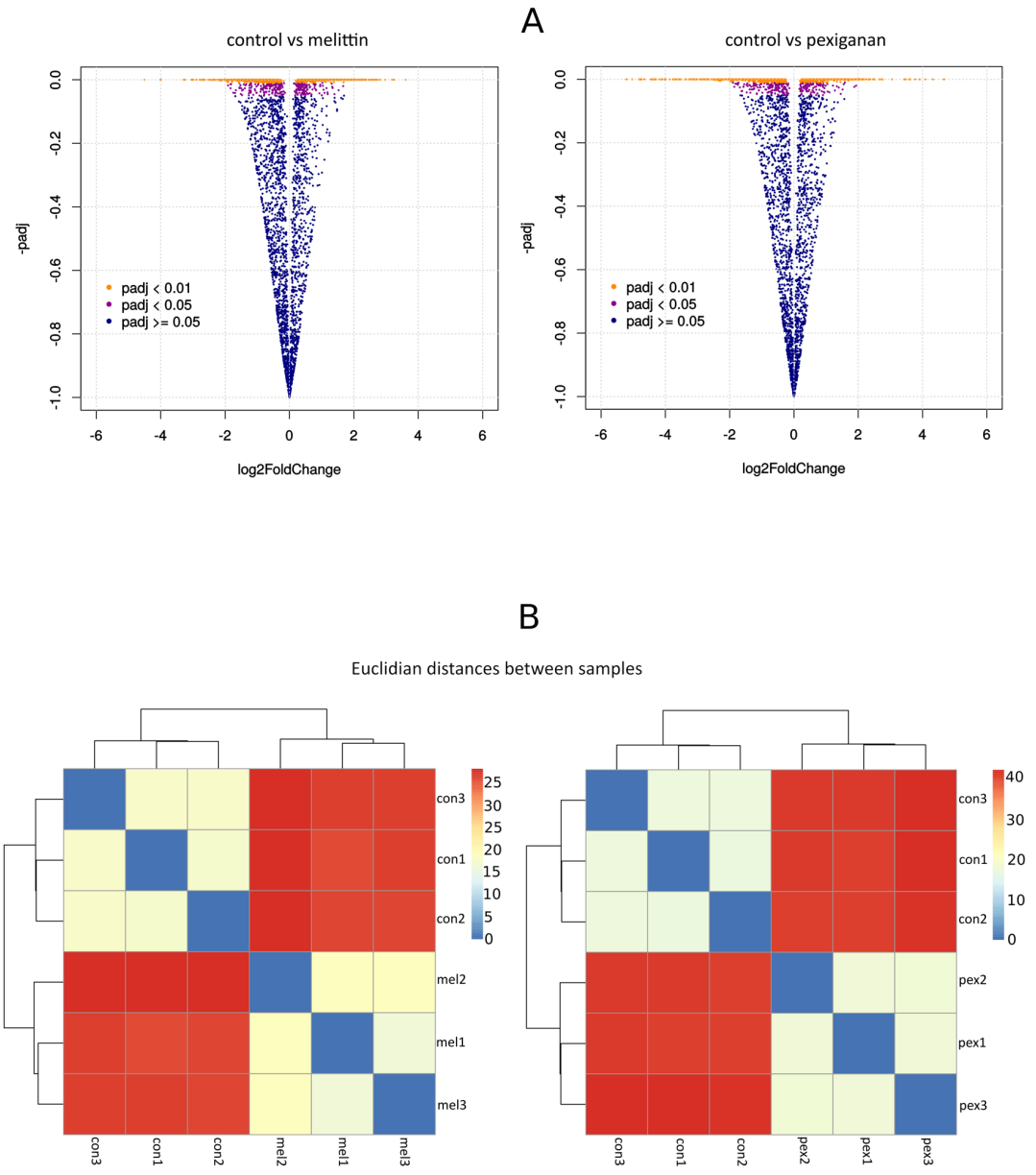

Figure S 18. Quality control of RNA sequencing by evaluating symmetry and distribution of the transcriptome counts, volcano plots showing different degrees of significance (A) and assessing dissimilarities of sample-based Euclidian hierarchical clustering for cells treated with priming

concentrations of melitting and pexiganan (B). Datasets are based on RNAseq of three independent biological replicas.

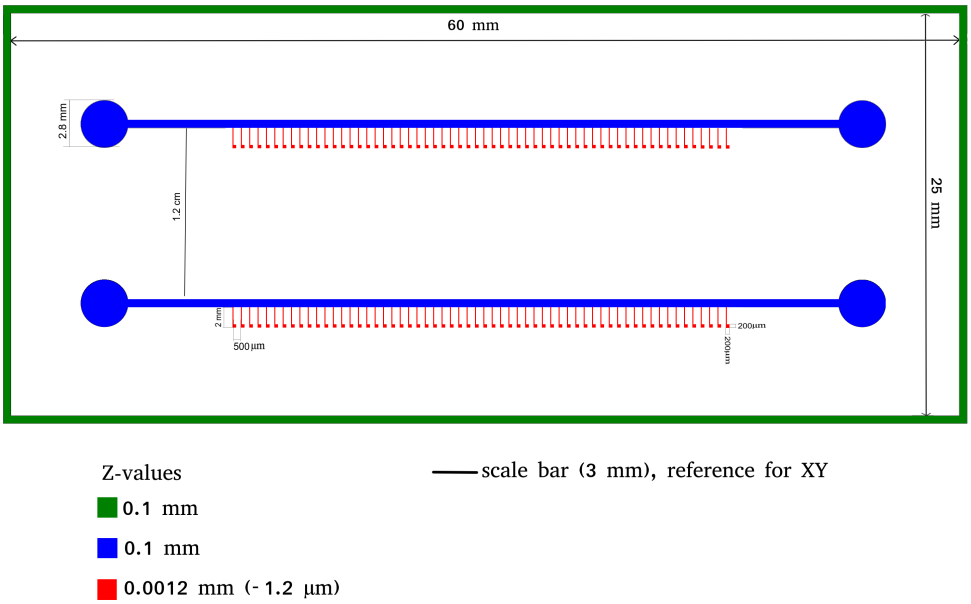

Figure S 19. Microfluidic device design used for live imaging of priming and killing of *E. coli* MG1655 by AMPs. Z-values refers to the depth of chip features while X and Y represent the dimensions of 2D axes. Each chamber square compartment was designed to be similar in size (200 µm) to a microscope field with a magnification of 1000X.